

# Incorporating GNSS Information with LIDAR-Inertial Odometry for Accurate Land-Vehicle Localization

Jintao Cheng<sup>1</sup>, Bohuan Xue<sup>1</sup>, Shiyang Chen<sup>2</sup>, Qiuchi Xiang<sup>1</sup> and Xiaoyu Tang<sup>1</sup>✉

**Abstract**—Currently, visual odometry and LIDAR odometry are performing well in pose estimation in some typical environments, but they still cannot recover the localization state at high speed or reduce accumulated drifts. In order to solve these problems, we propose a novel LIDAR-based localization framework, which achieves high accuracy and provides robust localization in 3D pointcloud maps with information of multi-sensors. The system integrates global information with LIDAR-based odometry to optimize the localization state. To improve robustness and enable fast resumption of localization, this paper uses offline pointcloud maps for prior knowledge and presents a novel registration method to speed up the convergence rate. The algorithm is tested on various maps of different data sets and has higher robustness and accuracy than other localization algorithms.

## I. INTRODUCTION

Accurate localization is a crucial component of Autonomous driving [1], [2]. Besides integrated navigation-based solutions, the main approaches include LIDAR-based localization [8]–[10] and Vision-based localization [11]–[13]. LIDAR-based schemes are mainly based on the pointcloud registration, which can be solved via iterative closest point (ICP) method [5]. The ICP algorithm is effective, but may suffer from local minima in the face of sophisticated environments [4]. Integrated Navigation-based methods can obtain high-precision global localization, while it often fails in complex urban environments. Furthermore, vision-based solutions are usually used in indoor environments because cameras are subject to interference from sunlight and rainy. Therefore, such methods may produce large cumulative errors.

Among the different challenges involved, LIDAR-based localization exhibits high robustness and accuracy. In the case of pure LIDAR-based odometry, the method in [10] scores among the highest in terms of translational and rotational errors on the Kitti Vision Benchmark [14]. However, in the environment of long trajectory and geometric degradation, LIDAR odometry will generate accumulated errors and drift without a prior pointcloud map. In particular, other sensors need to be used to finish re-localization after the localization has been lost for a long time. On the other side, LIDAR registration [15], [20] (alignment with respect to the offline 3D pointcloud maps) can provide high-precision localization and solve the accumulated errors and drift to a certain extent, while common registration algorithms are difficult to realize real-time analysis [27], [28].

Based on the above issues, we apply a sensor fusion framework to correct the accumulated error and accelerate the re-localization in the odometry. The framework realizes robust and high accurate localization between the online and a prior offline 3D pointcloud map. Compared with SLAM methods, our method uses the prior pointcloud map to make the whole localization system more robust. It also combines IMU with GNSS sensor to improve the global positioning accuracy and the relative positioning stability, so that it can compensate for the slow operation of the registration algorithm.

Our main contribution is proposing a robust sensor fusion localization framework, which can provide robust localization. In the complex urban environment, we perform pose optimization estimation by combining GNSS, IMU, and LIDAR. Compared with other localization frameworks, we use a prior map to complete pointcloud registration, which undoubtedly improves the stability of the system. Meanwhile, in order to improve the accuracy and efficiency of pointcloud registration, we propose an innovative registration algorithm Dynamic-ICP. Finally, we propose a mechanism using multi-sensor information to judge whether the registration fails.

The main contributions of this paper are summarized as follows:

- 1) We present a robust localization system in a prior 3D feature map, which combines a GNSS-based global odometry and an optimized LIDAR-Inertial odometry.
- 2) We propose a novel Dynamic-ICP registration method, which is employed in the LIDAR odometry, to solve the re-localization problem and enhance localization accuracy.
- 3) We apply a constrained GNSS velocity-aided pose adjustment method to estimate the heading and help the system perform more accurate localization.

## II. RELATED WORK

Both camera and LIDAR are fundamental sensors, which are crucial for autonomous localization problems. The relevant scientific research work can be divided into two subparts addressed in this paper. The characteristic of high frequency and low cost make Vision-based localization become one of the research directions. The works that are closely related to the method shown in this paper are LIDAR-based localization. In this section, we will briefly introduce state-of-the-art work in the field of Vision-based localization and LIDAR-based localization.

<sup>1</sup> South China Normal University

<sup>2</sup> Charles III University of Madrid

Corresponding author: Xiaoyu Tang: tangxy@scnu.edu.cn.

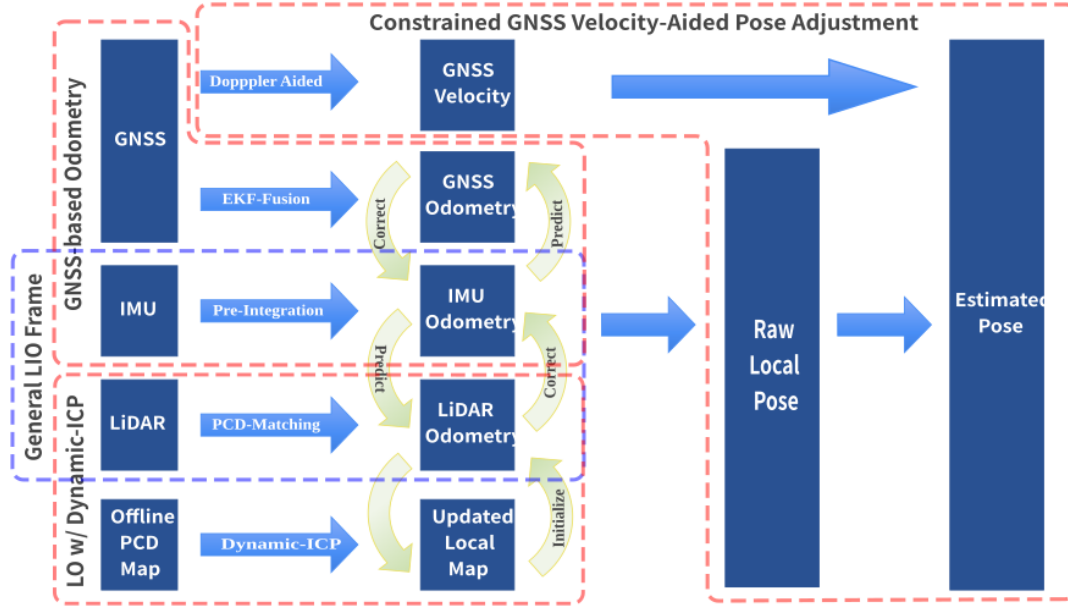


Fig. 1. The diagram of our method scheme. The red dotted box shows our three main sub-frameworks, and the blue dotted box shows the general LIO frame.

#### A. Vision-based localization

Vision-based localization can be grouped under the three sub-methods including feature-based method, direct method, and semi-direct method. [12] shows a feature-based method that uses various cameras and [11] presents a robust and versatile monocular visual-inertial state estimator. Because the camera is easy to be affected by a wide range of illumination angles, the feature point method is not suitable for some repeated texture or weak texture environments. In [21], previous researchers propose a visual odometry based on a direct structure and motion formulation. Although it can solve the localization problem in a weak texture environment, its characteristics make it unable to complete re-localization. In [13], a semi-direct method, which uses intensity gradients to track and joint feature points optimization, has been proposed. Using different methods in visual odometry have various advantages, but it usually performs not well enough in complex environments.

#### B. LIDAR-based localization

In recent years, LIDAR-based approaches have developed rapidly. Apart from the classical point-to-point error terms, there have been many error metrics proposed for the ICP mapping. For instance, the point-to-line and point-to-plane metrics are now benefiting the robotics community from their highly accurate pointcloud mapping. However, these new metrics are more challenging since the induced problems are non-convex in terms of the rotation and translation, thus many efforts are paid to give efficient and accurate

globally optimal solutions [3]. Compared to classical algorithm [10], [22], [23] propose LIDAR Odometry based on graph optimization to achieve trajectory estimation and map-building. This method is generally used to build maps, but the computation is usually inefficient. [30] propose a method of pre-tracker, which allows to obtain pre-computed odometry, to be used as aids when performing tracking. Pointcloud registration methods to estimate pose are presented in [15], [20]. In [8], the authors introduce a fast direct localization in 3D pointcloud maps without features and point correspondences, while its method can not get the initial pose. [9] shows a localization method joint LIDAR-Odometry [10] and scene recognition. Because segmentation is used in this algorithm, it needs to occupy computer graphics card resources. Despite the success of these methods, all the aforementioned methods do not complete the initial localization and re-localization on the pointcloud map, which means that their stability is questionable.

#### C. Pointcloud Map based localization

Based on the above method, some literatures use a prior map for localization. [17], [18] utilize features of the pointcloud maps in their visual system which can provide the accurate estimation of global 6-DoF camera poses with the absolute scale. Similarly, LIDAR-based localization makes use of the prior maps such as [8], [9], [19] to improve robustness. It can be seen that the constraints of pointcloud maps play a great role in improving the accuracy and robustness of localization.

### III. SYSTEM FRAMEWORK

#### A. System Review

The flowchart of the proposed method is shown in Fig. 1. We take the LIDAR as the global coordinate system and convert the external parameters of GNSS and IMU to the LIDAR coordinate system according to the known parameters.

We introduce three odometry modules, including GNSS-based odometry, IMU-preintegration odometry, and LIDAR-based odometry into the localization framework. The GNSS-based Odometry provides global localization for initializing or restarting the entire system framework. The system uses Pre-integration odometry as motion prediction and joint LIDAR-based odometry while optimizing the poses. The LIDAR odometry employs our dynamic-ICP algorithm for initial localization or re-localization, but in other cases, the IMU prior information is utilized to accelerate the iterative optimization of ICP.

Meanwhile, this framework relies on a prior 3-D pointcloud map, which supports a variety of mapping algorithms. In the process of localization, the algorithm generates local maps according to the current pose set to improve the matching efficiency. Then, the robustness of frame localization in various algorithms will be presented in the next part.

#### B. GNSS-based Odometry

Although GNSS is greatly affected by the urban environment, it can supply reliable global information for the system. Compare to the optimization-based method [24] [23], filter-based method [25] [26] have the advantages of small amount of calculation and strong real-time performance. Since global odometry is only used for system initialization or restart, we use EKF [29] as the fusion method. It is a practical approach to use high-frequency IMU to complete the prediction process and low-frequency GNSS to correct.

$$\mathbf{x} = (\phi, \theta, \psi, P_e, P_n, h_{\text{MSL}}, \mathbf{V}_e, \mathbf{V}_n, \mathbf{V}_u)^\top \quad (1)$$

$\mathbf{x}$  is the output of state variance, where  $\phi, \theta$  and  $\psi$  represents three axis attitude angle. Let  $P_e, P_n, h_{\text{MSL}}, \mathbf{V}_e, \mathbf{V}_n$  and  $\mathbf{V}_u$  define as three axis pose and velocity in ENU coordinate system.

$$\mathbf{z} = (\psi_{\text{mag}}, P_{e,g}, P_{n,g}, h_{\text{MSL},g}, \mathbf{V}_{e,g}, \mathbf{V}_{n,g}, \mathbf{V}_{u,g})^\top \quad (2)$$

Where  $\mathbf{z}$  is defined as the measurement variance, and  $\psi_{\text{mag}}$  is magnetometer measurement. GNSS provides there axis position  $P_{e,g}, P_{n,g}, h_{\text{MSL},g}$  and three axis velocity  $\mathbf{V}_{e,g}, \mathbf{V}_{n,g}, \mathbf{V}_{u,g}$ .

#### C. IMU-preintegration Odometry

We maintain an odometer based on IMU pre-integration [16] as the initial value of pointcloud registration. The raw measurements of the IMU are defined using Eqs. 1 and 2.

$$\hat{\omega}_k = \omega_k + \mathbf{b}_k^\omega + \mathbf{n}_k^\omega \quad (3)$$

$$\hat{\mathbf{a}}_k = \mathbf{R}_k^{-1} (\mathbf{a}_k - \mathbf{g}) + \mathbf{b}_k^a + \mathbf{n}_k^a \quad (4)$$

where, letting the current timestamp as  $k$ ,  $\hat{\omega}_k$  is the raw angular velocity with bias  $\mathbf{b}_k^\omega$  and noise  $\mathbf{n}_k^\omega$  in the time  $k$ ;  $\hat{\mathbf{a}}_k$  is the raw acceleration with bias  $\mathbf{b}_k^a$  and noise  $\mathbf{n}_k^a$ ;  $\mathbf{R}_k^{-1}$  is the rotation matrix from world coordinate system to body coordinate system;  $\mathbf{g}$  is the constant gravity vector in world coordinate system.

Using the pre-integration method can obtain the relative body motion between two timestamps. The increments of displacement, velocity, and rotation in time  $i$  and  $j$  can be calculated as

$$\Delta \mathbf{v}_{ij} = \mathbf{R}_i^\top (\mathbf{v}_j - \mathbf{v}_i - \mathbf{g} \Delta k_{ij}) \quad (5)$$

$$\Delta \mathbf{p}_{ij} = \mathbf{R}_i^\top \left( \mathbf{p}_j - \mathbf{p}_i - \mathbf{v}_i \Delta k_{ij} - \frac{1}{2} \mathbf{g} \Delta k_{ij}^2 \right) \quad (6)$$

$$\Delta \mathbf{R}_{ij} = \mathbf{R}_i^\top \mathbf{R}_j \quad (7)$$

Let  $\mathbf{v}_k$  defines as the velocity in time  $k$ ,  $\mathbf{p}_k$  represents the displacement in time  $k$ , where  $\mathbf{R}_k$  is the rotation in time  $k$ .

Due to the conversion  $\mathbf{T}_{l2m}$  between the IMU coordinate system and the LIDAR coordinate system, we can define the pose of the IMU odometry in the LIDAR coordinate system  $\mathbf{T}_{lidar}$  as

$$\mathbf{T}_{lidar} = \mathbf{T}_{l2m} \mathbf{T}_{imu} \quad (8)$$

#### D. LIDAR Odometry with Dynamic ICP

LIDAR Odometry plays a significant role in the whole localization framework. Before starting the LIDAR Odometry process, we would like to load the offline map which is used the state of the art mapping algorithms [10], [20], [23].

Algorithm 1 shows the Dynamic ICP Algorithm, which is a novel pointcloud registration algorithm to obtain fast and high accuracy localization in initial and re-localization. The odometry is calculated by the usage of a prior map and the current LIDAR frame, depending on the remarkable accuracy of ICP with a dynamic calculation and fast response. This method is able to apparently overcome the shortcomings of the normal ICP algorithm, the lack of costing such a long time, by setting the believable initial guess transformation between LIDAR frames and restricting the matching region as well.

The process of the algorithm will be divided into two parts, region selecting and ICP matching. The first step is to select a region of the local map for further matching. Due to the lack of finding the absolute position in the map frame, it is such a hard challenge for LIDAR to find out where it is in the global map frame for the first time. A commonly used method to solve this problem is to match the frame with frames at plenty of way-points, saved while building the map to make sure the maximum likely pose in the map. However, it will cost a long time to search through all of the possible areas. On the contrary to this method, our algorithm takes usage of GNSS messages as an observation globally to offer the initial guess, and select a local map around the guess position with a smaller range that gives a higher success rate for each attempt. Moreover, the region size can be adaptive

so as to make it effective in most scenes even if the GNSS data is not reliable enough.

---

**Algorithm 1** Dynamic ICP Algorithm

---

```

1: Initialization:  $T_{k,0} = [R_{k,0}, t_{k,0}; 0, 1]$ ,  $i \leftarrow 0$ ,
    $r_k \leftarrow \text{SCANRANGE}$  (via GNSS)
2:  $p_{k,0} = T_{k,0} \cdot p_{k-1}$ 
3: if  $\|pts_n^{gmap}, p_{k,0}\| < r_k$  then
4:    $pts_k^m \leftarrow pts_n^{gmap}$ 
5: end if
6:  $E(T_k) = \arg \min_{T_k \in SE3} \frac{1}{|pts^l|} \sum_{n=1}^{pts^l} pts_n^m - (t_k + R_k \cdot pts_n^l)$ 
7: repeat
8:    $i \leftarrow i + 1$ 
9:   Update  $T_{k,i}$  based on Equation (6)
10:  Update  $p_{k,i}$  based on Equation (4)
11: until  $E(T_k) < \text{Error Tolerance}$ 
12:  $T_k = T_{k,i}$ 
13:  $p_k = p_{k,i}$ 
Output: transformation matrix  $T_k$  & current pose  $p_k$ 

```

---

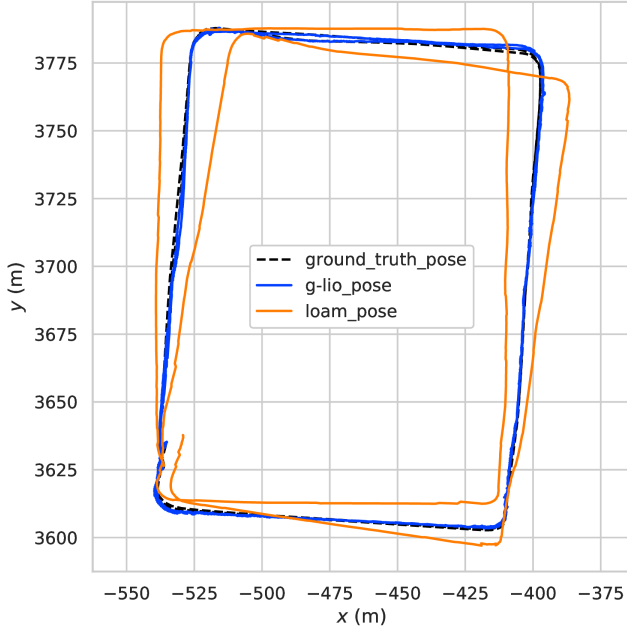


Fig. 2. Comparison of trajectory results of our method, LOAM and ground truth in HK02 [7] dataset.

### E. Constrained GNSS Velocity-Aided Pose Adjustment

We use an indirect Kalman filter (IKF) to estimate the heading, pitch angles along with non-gravitational acceleration with the GNSS velocity. It runs with a relatively low sampling rate (typical time period: 1 s). It substantially plays an important role in correcting systematic errors of MARG sensors. More importantly, the GNSS velocity vector contains information of pitch and yaw, with roll to be an undetermined stated in the Kalman filter. In this way, a constrained IKF is proposed to constrain the roll angle

during the propagation of Kalman filtering. We use the error quaternion representation to propagate the IKF. The error quaternion is defined as  $\hat{q}_{e,k} = (1, \mathbf{y}_k^\top)^\top$  in the time instant  $k$ , with error term  $\mathbf{y}_k$  being the state vector of the IKF. The quaternion is propagated using.

$$\hat{q}_{k+1} = \frac{\hat{q}_k \odot \hat{q}_{e,k}}{\|\hat{q}_k \odot \hat{q}_{e,k}\|} \quad (9)$$

With (9),  $R_n^b$  at time  $k$  is renewed with  $\hat{q}_k$  and the initial value of  $\hat{q}_{e,k}$  is reset as zero. Thus for the IKF, its predicted state is computed by previous LIDAR odometry, with covariance of  $P_k$ . The observation model is written as

$$\tilde{w}_{v,k} = H_{v,k} \mathbf{y}_k + \varepsilon_s \quad (10)$$

where

$$\tilde{w}_{v,k} = w_{v,k} - R_n^b(\hat{\mathbf{y}}_{\text{LIDAR},k}) \mathbf{v}^n$$

$$H_{v,k} = 2 \left[ (R_n^b(\hat{\mathbf{y}}_{\text{LIDAR},k}) \mathbf{v}^n) \times \right].$$

However, as is well understood, velocity generated from a single antenna GNSS does not provide any roll information itself. In such point of view, we conduct a roll-constraint based IKF. Defining the IKF estimate of quaternion error as  $\hat{q}_{e,v,k}$ , then the final rotation matrix is obtained through

$$R_n^b(\hat{q}_{v,k}) = R_n^b(\hat{q}_{e,v,k}) R_n^b(\hat{q}_k) \quad (11)$$

where

$$R_n^b(\hat{q}_{e,v,k}) = \begin{bmatrix} 1 & 2\hat{\mathbf{y}}_k(3) & -2\hat{\mathbf{y}}_k(2) \\ -2\hat{\mathbf{y}}_k(3) & 1 & 2\hat{\mathbf{y}}_k(1) \\ 2\hat{\mathbf{y}}_k(2) & -2\hat{\mathbf{y}}_k(1) & 1 \end{bmatrix}$$

and  $\hat{\mathbf{y}}_k(i)$  for  $i = \{1, 2, 3\}$  denotes the  $i$ -th element of IKF estimate  $\hat{\mathbf{y}}_{v,k}$ .

Considering roll constraint of attitude quaternion, we have

$$f(\hat{q}_{e,v,k}) = \frac{[R_n^b(q_k)]_{(2,3)}}{[R_n^b(q_k)]_{(3,3)}} - \frac{[R_n^b(\hat{q}_{\text{LIDAR},k})]_{(2,3)}}{[R_n^b(\hat{q}_{\text{LIDAR},k})]_{(3,3)}} = 0 \quad (12)$$

Referring to (12), this constraint indicates that the IKF does not exert any roll correction on the previous solution. Inserting (11) into (12) yields an equality

$$\Theta_k^\top \hat{\mathbf{y}}_k = 0 \quad (13)$$

where  $\Theta_k$  is given by (??). The following optimization problem is constructed with

$$\arg \min_{\hat{\mathbf{y}}_k} \frac{1}{2} \mathbf{V}_k^\top \Sigma_v^{-1} \mathbf{V}_k, \quad \text{s.t.} \quad \Theta_k^\top \hat{\mathbf{y}}_k = 0 \quad (14)$$

where  $\mathbf{V}_k$  is the residual for observation model,

$$\mathbf{V}_k = H_{v,k} \hat{\mathbf{y}}_k - \tilde{w}_{v,k} \quad (15)$$

Introducing the Lagrange multiplier  $\lambda$  gives the Lagrangian of

$$\mathcal{L} = \frac{1}{2} \mathbf{V}_k^\top \Sigma_v^{-1} \mathbf{V}_k + \lambda \Theta_k^\top \hat{\mathbf{y}}_k \quad (16)$$

Evidently,  $\mathcal{L}$  is a convex and continuous function of  $\hat{\mathbf{y}}_k$  and  $\lambda$ . Taking the derivative of  $\mathcal{L}$  with respect to  $\hat{\mathbf{y}}_k$  and  $\lambda$ , we obtain the gradient

$$\begin{aligned}\nabla \mathcal{L}_{\mathbf{y}} &= \mathbf{H}_{v,k}^\top \Sigma_v^{-1} (\mathbf{H}_{v,k} \hat{\mathbf{y}}_k - \tilde{\mathbf{w}}_{v,k}) + \lambda \Theta_k \\ \nabla \mathcal{L}_{\lambda} &= \Theta_k^\top \hat{\mathbf{y}}_k\end{aligned}\quad (17)$$

Zeroing the gradient gives solution to  $\hat{\mathbf{y}}_k$ , which is in the form of a linear system that is easy to be solved.

#### F. LIDAR-Inertial-GNSS Integrated Navigation

To solve the drawback of low frequency LIDAR Odometry, jointing IMU Odometry is an efficient method. We use the quadratic curve approximate interpolation method to fuse the output of IMU and LIDAR. Let the result output is  $Q^l$ .

In order to enhance the system robustness, we utilize GNSS information to optimize. The optimization formula is as follows, where  $\alpha$ ,  $\beta$  and  $A$  are super parameters. Let  $\mathbf{V}_g$  defines as GNSS velocity, where  $\Delta \mathbf{Q}_l$  is the relative pose between timestamp  $t$  and  $t-1$ ,  $\mathbf{Q}_t$  and  $\mathbf{Q}_{t-1}$  is the IMU and lidar fused output in timestamp  $t$  and  $t-1$ .  $\Xi$  represents the matrix of GNSS covariance.  $\mathbf{Q}_t^g$  is defined as GNSS-based Odometry in the timestamp  $t$ .

$$\hat{\mathbf{Q}} = \begin{cases} (1 - \beta) \int_{\Delta t} \mathbf{V}_g + \beta \Delta \mathbf{Q}^l + \mathbf{Q}_{t-1}^l & \text{tr}(\Xi) > A \\ (1 - \alpha) \mathbf{Q}_t^g + \alpha \mathbf{Q}_t' & \text{tr}(\Xi) \leq A \end{cases} \quad (18)$$

The trace of the covariance matrix of GNSS reflects the current position degradation degree to a certain extent. When the trace is greater than  $A$ , the GNSS position information has a certain degradation, and the effectiveness of the current GNSS based data is reduced, but the velocity information integral of GNSS can be used for fusion. When the trace is less than  $A$ , the fusion of GNSS odometry can well correct the cumulative drift of odometry.

#### IV. EXPERIMENTAL RESULTS

We carry out experiments on a system equipped with an Intel i7-9700 processor, with 32Gb of RAM in all experiments. Prior pointcloud maps are built in all sequences with various mapping algorithms to test localization accuracy.

Here are our test results on public dataset HK01, HK02 [7], and KITTI18, KITTI28 [14]. We tested our algorithm on these dataset with the comparison of other widely used SLAM methods, including [10] [5] [20]. The mainly used indicator for evaluating the efficiency in this section is Root Mean Square Error(RMSE). The results show that our method performs better than the base methods, and the data of experiments are shown detailedly in TABLE I.

#### V. CONCLUSIONS

At high speeds, commonly used LIDAR and visual odometry systems produce accumulated drift that is difficult to eliminate. Additionally, there has been a lack of fast re-localization methods when the predicted pose is inaccurate. Our proposed framework introduces three odometry

TABLE I  
RMSE EXPERIMENT RESULTS TABLE ON DIFFERENT DATASET

Sequence	MAP_METHOD	LOAM <sup>1</sup>	ICP	NDT	OURS
HK01	NDT-MAPPING	4.57	2.00	3.13	<b>1.98</b>
	LEGO_LOAM		4.34	5.50	<b>1.96</b>
HK02	NDT-MAPPING	31.69	0.88	0.92	<b>0.77</b>
	LEGO_LOAM		1.17	1.13	<b>1.08</b>
KITTI18	NDT-MAPPING	18.00	X <sup>2</sup>	3.62	<b>0.99</b>
	LEGO_LOAM		X	3.92	<b>1.22</b>
KITTI28	NDT-MAPPING	32.00	X	9.66	<b>1.98</b>
	LEGO_LOAM		X	8.00	<b>2.24</b>

<sup>1</sup> The LOAM method used odometers directly and was independent of how the map is constructed.

<sup>2</sup> The ICP method does not run completely on the KITTI dataset, so its RMSE is not calculated in this paper.

modules, including GNSS-based odometry, which provides reference values for LIDAR-inertial odometry at a relatively low sampling frequency by introducing GNSS velocity and pose information, as well as IMU pre-integrated odometry and LIDAR-based odometry. Moreover, in order to solve the re-localization problem, we propose the Dynamic-ICP method, which selects the most likely suitable size area in the local map through the area selection algorithm to improve the convergence speed of point cloud registration and re-localization accuracy. In other cases, The system uses pre-integrated odometry as motion prediction to joint lidar-based odometry while optimizing poses, and IMU priors are used to speed up the iterative optimization of pointcloud matching. Since an offline 3-D pointcloud map is needed by our framework, it is designed to adapt maps generated by the most commonly used mapping algorithms. Through experimental comparisons, it can be seen that the algorithm remains stable in various complex environments and both single-Lidar and multi-Lidar platforms. In future work, we plan to add more sensor information, such as GNSS raw data, to update our positioning framework.

#### REFERENCES

- [1] J. Cheng, K. Zeng, Z. Huang, X. Tang, J. Wu, C. Zhang, X. Chen, and R. Fan, "Mf-mos: A motion-focused model for moving object segmentation," in *2024 IEEE International Conference on Robotics and Automation (ICRA)*, 2024, pp. 12 499–12 505.
- [2] M. Jia, Q. Zhang, B. Yang, J. Wu, M. Liu, and P. Jensfelt, "BeautyMap: Binary-encoded adaptable ground matrix for dynamic points removal in global maps," *IEEE Robotics and Automation Letters*, vol. 9, no. 7, pp. 6256–6263, 2024.
- [3] J. Wu, Y. Zheng, Z. Gao, Y. Jiang, X. Hu, Y. Zhu, J. Jiao, and M. Liu, "Quadratic Pose Estimation Problems : Globally Optimal Solutions , Solvability / Observability Analysis and Uncertainty Description," *IEEE Trans. Robot.*, pp. 1–20.
- [4] H. Yang, J. Shi, and L. Carlone, "TEASER: Fast and Certifiable Point Cloud Registration," *IEEE Trans. Robot.*, pp. 1–20, 2020.
- [5] P. J. Besl and N. D. McKay, "A Method for Registration of 3-D Shapes," *IEEE Trans. Pattern Anal. Mach. Intell.*, vol. 14, no. 2, pp. 239–256, 1992.
- [6] M. Schreiber, C. Knoppel, and U. Franke, "Laneloc: Lane marking based localization using highly accurate maps," in *Intelligent Vehicles Symposium (IV)*, 2013 IEEE, 2013.

- [7] L.-T. Hsu, N. Kubo, W. Wen, W. Chen, Z. Liu, T. Suzuki, and J. Meguro, "Urbannav: An open-sourced multisensory dataset for benchmarking positioning algorithms designed for urban areas," in *ION GNSS+ 2021*, 2021, pp. 226–256.
- [8] F. Caballero and L. Merino, "Dll: Direct lidar localization. a map-based localization approach for aerial robots," in *2021 IEEE IROS*, 2021, pp. 5491–5498.
- [9] D. Rozenberszki and A. L. Majdik, "Lol: Lidar-only odometry and localization in 3d point cloud maps\*," in *2020 IEEE ICRA*, 2020, pp. 4379–4385.
- [10] Z. Ji and S. Singh, "Loam: Lidar odometry and mapping in real-time," in *Robotics: Science and Systems Conference*, 2014.
- [11] T. Qin, P. Li, and S. Shen, "Vins-mono: A robust and versatile monocular visual-inertial state estimator," *IEEE Trans. Robot.*, vol. 34, no. 4, pp. 1004–1020, 2018.
- [12] R. Mur-Artal and J. D. Tardós, "Orb-slam2: An open-source slam system for monocular, stereo, and rgb-d cameras," *IEEE Trans. Robot.*, vol. 33, no. 5, pp. 1255–1262, 2017.
- [13] C. Forster, Z. Zhang, M. Gassner, M. Werlberger, and D. Scaramuzza, "Svo: Semidirect visual odometry for monocular and multicamera systems," *IEEE Trans. Robot.*, vol. 33, no. 2, pp. 249–265, 2017.
- [14] A. Geiger, P. Lenz, and R. Urtasun, "Are we ready for autonomous driving? the kitti vision benchmark suite," in *2012 IEEE CVPR*, 2012, pp. 3354–3361.
- [15] E. D. Recherche, E. E. Automatique, S. Antipolis, and Z. Zhang, "Iterative point matching for registration of free-form curves," *International Journal of Computer Vision*, vol. 13, 1992.
- [16] C. Forster, L. Carlone, F. Dellaert, and D. Scaramuzza, "supplementary material to: imu preintegration on manifold for efficient visual-inertial maximum-a-posteriori estimation," 2019.
- [17] H. Yu, W. Zhen, W. Yang, J. Zhang, and S. Scherer, "Monocular camera localization in prior lidar maps with 2d-3d line correspondences," in *2020 IEEE IROS*, 2020, pp. 4588–4594.
- [18] H. Ye, H. Huang, and M. Liu, "Monocular direct sparse localization in a prior 3d surfel map," in *2020 IEEE ICRA*, 2020, pp. 8892–8898.
- [19] Y. Zhu, B. Xue, L. Zheng, H. Huang, M. Liu, and R. Fan, "Real-time, environmentally-robust 3d lidar localization," in *2019 IEEE IST*, 2019, pp. 1–6.
- [20] P. Biber and W. Strasser, "The normal distributions transform: a new approach to laser scan matching," in *2003 IEEE IROS*, vol. 3, 2003, pp. 2743–2748 vol.3.
- [21] J. Engel, V. Koltun, and D. Cremers, "Direct sparse odometry," *IEEE Trans. Pattern Anal. Mach. Intell.*, vol. 40, no. 3, pp. 611–625, 2018.
- [22] T. Shan and B. Englot, "Lego-loam: Lightweight and ground-optimized lidar odometry and mapping on variable terrain," in *2018 IEEE IROS*, 2018, pp. 4758–4765.
- [23] T. Shan, B. Englot, D. Meyers, W. Wang, C. Ratti, and D. Rus, "Lio-sam: Tightly-coupled lidar inertial odometry via smoothing and mapping," in *2020 IEEE IROS*, 2020, pp. 5135–5142.
- [24] H. Ye, Y. Chen, and M. Liu, "Tightly coupled 3d lidar inertial odometry and mapping," in *2019 IEEE ICRA*, 2019, pp. 3144–3150.
- [25] S. Zhao, Z. Fang, H. Li, and S. Scherer, "A robust laser-inertial odometry and mapping method for large-scale highway environments," in *2019 IEEE IROS*, 2019, pp. 1285–1292.
- [26] G. Wan, X. Yang, R. Cai, H. Li, Y. Zhou, H. Wang, and S. Song, "Robust and precise vehicle localization based on multi-sensor fusion in diverse city scenes," in *2018 IEEE ICRA*, 2018, pp. 4670–4677.
- [27] S.-H. Chan, P.-T. Wu, and L.-C. Fu, "Robust 2d indoor localization through laser slam and visual slam fusion," in *2018 IEEE SMC*, 2018, pp. 1263–1268.
- [28] Q. Ye, L. Shu, and W. Zhang, "Extrinsic calibration of a monocular camera and a single line scanning lidar," in *2019 IEEE ICMA*, 2019, pp. 1047–1054.
- [29] J. D. Barton, "Fundamentals of small unmanned aircraft flight," *Johns Hopkins Apl Technical Digest*, vol. 31, no. 2, pp. 132–149, 2012.
- [30] M. Frosi and M. Matteucci, "ART-SLAM: accurate real-time 6dof lidar SLAM," *CoRR*, vol. abs/2109.05483, 2021. [Online]. Available: <https://arxiv.org/abs/2109.05483>
- [31] J. Jiao, Q. Liao, Y. Zhu, T. Liu, Y. Yu, R. Fan, L. Wang, and M. Liu, "A novel dual-lidar calibration algorithm using planar surfaces," 2019.
- [32] J. Lv, J. Xu, K. Hu, Y. Liu, and X. Zuo, "Targetless calibration of lidar-imu system based on continuous-time batch estimation," in *2020 IEEE IROS*, 2020, pp. 9968–9975.
- [33] C. Chen, G. Xiong, Z. Zhang, J. Gong, J. Qi, and C. Wang, "3d lidar-gps/imu calibration based on hand-eye calibration model for unmanned vehicle," in *2020 3rd ICUS*, 2020, pp. 337–341.